IOP Conf. Series: Materials Science and Engineering **249** (2017) 012005 doi:10.1088/1757-899X/249/1/012005

Parametric Optimization of Multi-Electrode Plasma Actuator with Serrated Electrode

T Matsuno[1], A Fukuda[1], H Kawazoe[1], K Nakai[2] and H Nishida[3]

[1] Department of Mechanical and Aerospace Engineering, Tottori University, Tottori, Tottori 680-8550, Japan
[2] Department Mechanical Systems Engineering, Tokyo University of Agriculture and Technology, Koganei, Tokyo 184-8588, Japan
[3] Institute of Engineering, Tokyo University of Agriculture and Technology, Tokyo 184-8588, Japan

E-mail: matsuno@mech.tottori-u.ac.jp

Abstract. The thrust performance of the multi-electrode plasma actuator has been investigated and optimized in terms of the configuration of the actuator element and the driving conditions, from the viewpoint of electrical mobility of ions. A trielectrode plasma actuator that has two exposed electrodes with serration in bilateral symmetry was used in this study. The induced body force of the plasma actuator was investigated on quiescent air, by measuring thrust of the induced jet. With the experimental results, the physical factors that affect the growth of thrust is considered, by estimating total momentum of ions from their drift velocity.

1. Introduction

Single dielectric barrier discharge (SDBD) plasma actuator, a flow control device that utilizes dielectric barrier discharge to generate wall-jet flow, demonstrate their potential in delaying separation and significant improvement in aerodynamic performances [1-3]. At the same time, due to the limitation of the physical mechanism of dielectric barrier discharge, it is difficult to increase plasma density to enhance the body force of the SDBD jet. In order to solve this problem, several types of the plasma actuators which derived from standard SDBD type have been proposed and developed.

One promising approach is the use of additional electrode to enhance discharge and assist acceleration of the generated ions from that discharge. Sosa et al. have tested a multi-electrode plasma actuator that has additional electrode to apply DC voltage [4, 5]. This type of the device is called trielectrode (TED) plasma actuator. The basic SDBD plasma actuator would consist of a pair of electrodes isolated by a dielectric material. One of the electrodes is exposed to the air and the other is buried in a dielectric material so never contacts to the air. The electrodes are arranged in a staggered manner that shares a single edge, as shown in figure 1(a). Figure 1(b) shows the general configurations of the trielectrode plasma actuator. We call the additional exposed electrode as "DC electrode" in this paper. The original exposed electrode for applying AC voltage is called as "AC electrode" to prevent confusion.

Characteristics of the TED plasma actuator have been investigated on the electric aspect [6] and improvement of tangential thrust compared to SDBD plasma actuator [7, 8]. These researches clarified that TED plasma actuator could induce a jet with more than ten times larger thrust compared to a SDBD plasma actuator at same AC voltage. The application of DC voltage extends the ionization region and produce counter jet at the edge of the DC electrode. The interaction of these jets results an upward vectored jet. In order to understand the working mechanism of TED plasma actuator with DC high voltage, Nishida et al. conducted numerical simulation for plasma and induced flow. Figure 2 shows the time variation of plasma distribution for the case of positive DC voltage application obtained by numerical simulation [9]. In this case, the electrons produced from the AC discharge are attracted by the DC electrode, then they trigger the ionization to generate positive ions at the DC electrode. The drift motion of the generated positive ions results in the negative body force. These results indicated that the distance between the exposed electrodes and AC voltage frequency should have a strong impact on the body force produced from the TED plasma actuator, since the number of electrons and the drift velocity of ions are determined by these parameters.

In this research, the impact of the frequency of the AC voltage and the distance between their exposed electrodes on the thrust characteristics of the TED plasma actuator has been estimated by using a simple model and investigated by the experiment.

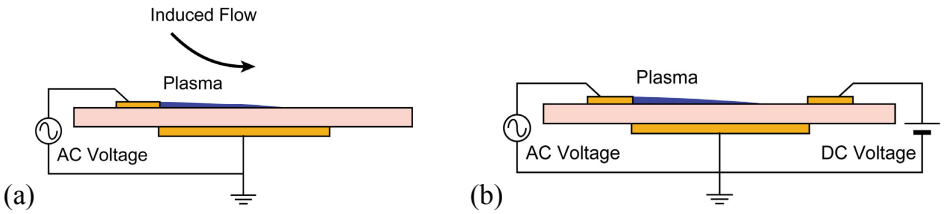

Figure 1. Schematic configurations of SDBD and the trielectrode plasma actuators: (a) SDBD plasma actuator, (b) Trielectrode plasma actuator.

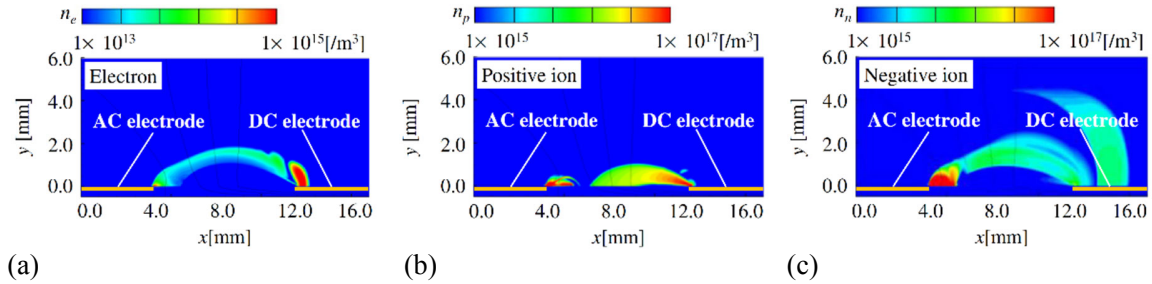

Figure 2. Time variation of the plasma distribution for the case of the DC voltage of 13.2 kV at a negative-going voltage half cycle: (a) electron density, (b) positive ion density, and (c) negative ion density [9].

2. Experimental setup

2.1. Plasma actuator

In this research, a trielectrode plasma actuator with serrated electrodes has been employed for experiment. The example image of the actuator and its serrated electrode are shown in figures 3 and 4. In this research,

the distance between vertexes of the triangle, d_s, was fixed at 1mm. Other dimensions and specifications of the plasma actuator employed in this work are summarized in Table 1.

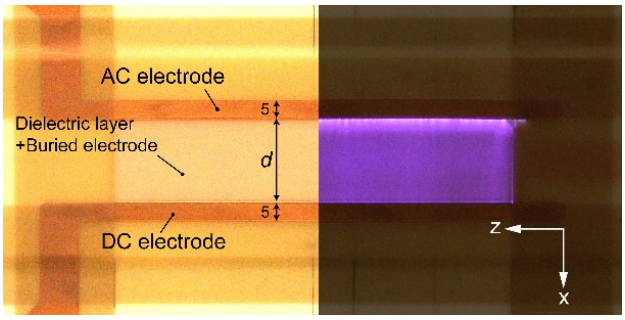

Figure 3. Photograph of the trielectrode plasma actuator element and its discharge.

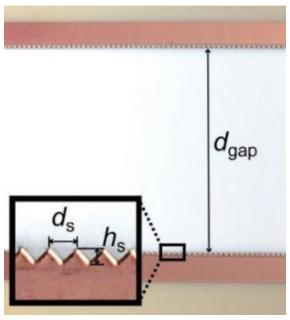

Figure 4. Image of the serrated exposed electrodes (triangular, 1mm spacing).

Table 1. Experimental conditions for thrust test of the trielectrode plasma actuator.

AC frequency: f_{ac}	4 ~ 18 kHz
AC voltage: V_{ac}	15.6 kVpp
DC voltage: V_{dc}	0 ~ 30.0 kV
Electrode material	Copper
Dielectric layer material	PTFE
Dielectric layer thickness	2 mm
Buried electrode width (Gap length): d_{gap}	40 ~ 80 mm
Exposed electrode width	5 mm
Overlap of electrodes	0 mm
Discharge length	200 mm
Distance between vertexes of serration: d_s	1 mm
Height of serration: h_s	0.5 mm

2.2. Power supply

Figure 5 shows a schematic of the power supply of plasma actuator used in this study. A reference waveform of a high-voltage AC input was generated by a function generator and amplified by a solid-state high power amplifier, which increases input power up to 400 W, with the amplitude of 70 V_{pp}. By a high voltage transformer, the AC voltage attains amplitude up to 30 kV at a frequency of 4 ~ 18 kHz. The voltage and current of AC input was monitored by a digital oscilloscope. DC voltage was applied directly from the high voltage power supply (Matsusada Precision HAR 30), which can generate up to 30 kV with 10 mA of output.

2.3. Thrust measurement

In this research, the thrust of the induced jet by the plasma actuator was measured, as a reaction of the aerodynamic force from the actuator, and was evaluated as an index of the flow control performance. The schematic of the apparatus for the thrust measurement is illustrated in figure 6. The thrust from plasma actuator was sensed by an analytical balance (Shimadzu AUW320) with a lever. Since the TED plasma actuator generates vectored jet, we need to measure the magnitude of the thrust and their angle.

In this experiment, two types of mounting base for actuator element were used to measure horizontal (tangential to the actuator surface) and vertical (perpendicular to the surface) thrust component separately, as shown in figure 6(a) and 6(b). The direction of the horizontal thrust was set as same as the thrust generated by SDBD actuator. The reference of the thrust was set at the centerline of exposed electrodes on the dielectric surface.

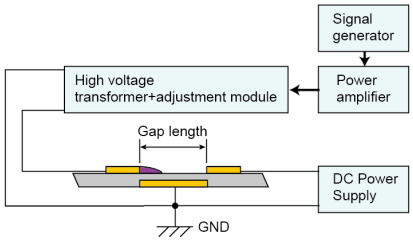

Figure 5. Connection diagram of the power supply for TED plasma actuator.

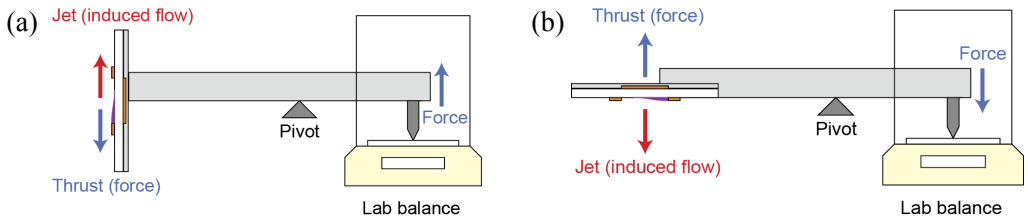

Figure 6. Schematics of thrust measurement system: (a) horizontal thrust measurement, (b) vertical thrust measurement.

3. Results and discussion

3.1. Estimating momentum of ions from drift velocity

The physical factors that affect the body force from plasma actuator are considered. The fundamental physical mechanism to produce induced jet is the drift motion of ions from the discharge as shown in figure 7. The momentum transfer from the ions to the neutral molecules through collisions produces the body force which induces the fluid motion to generate jet. In this process, the body force must have a causal relation to the total momentum of drifting ions. The total momentum is the product of the total mass of the ions and their drift velocity. The total mass of the ions can be represented by a number of ions from discharge, and the number of ions has a linear relation with the number of micro-discharge in each AC cycle. The report pointed [9] that the number of the micro-discharge is a function of a rate of AC voltage change over time, dV_{ac}/dt.

For the drift velocity of ions, it can be calculated with ion mobility and the electric field strength, assuming uniform electric field;

$$v_{\mathrm{i}} = \mu_{\mathrm{i}} E$$

The magnitude of the electric field strength was estimated from the RMS of the electric field between the electrodes;

$$E_{RMS}[\mathrm{V/m}] = \sqrt{\frac{1}{T}\int_0^T \left(\sin \omega t - \frac{V_{\mathrm{dc}}}{V_{\mathrm{ac}}}\right) dt} \cdot \frac{V_{\mathrm{ac}}}{d_{\mathrm{gap}}}$$

The ion mobility is set to be constant; $\mu_i = 20.0/p$ $m^2V^{-1}s^{-1}$, where p is the ambient gas pressure (1.013×10^5 Pa).

Figure 8 shows the calculated contours of the momentum of ions. The magnitude of momentum was simply estimated from the production of the ion drift velocity, v_i, and the nominal rate of the AC voltage change dV_{ac}/dt. These were normalized by the maximum value in the calculated conditions. The increase in the frequency relates directly to the rate of the AC voltage change. The increase in dV_{ac}/dt causes a growth in the number of micro-discharge, which results the increase of the number of ions. Figure 9 shows the effect of the gap length on the drift velocity of ions at the same conditions. For the gap length, the smaller gap length makes higher electric field strength, which leads higher drift velocity of ions.

Figure 10 shows the estimated drift velocity plotted against the DC voltage for various gap lengths. The trend is as expected; the larger drift velocity can be achieved at the high DC voltage. The effect is primarily same as the reduction of the gap length. This simply interprets the mechanism to enhance the jet on the AC electrode at high DC voltage. The plot also presents the trend that the change in the drift velocity becomes small as the gap length increases, even in the high DC voltage region. This is because the impact of the difference in the gap length on the electric field is diminished at large gap length.

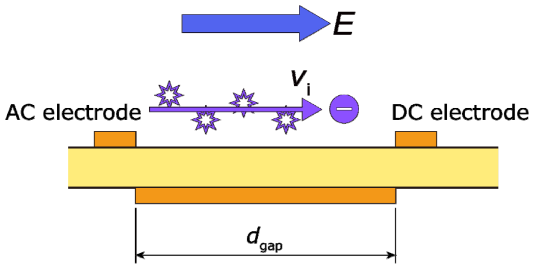

Figure 7. Schematic of ion drift between the exposed electrodes of trielectrode plasma actuator.

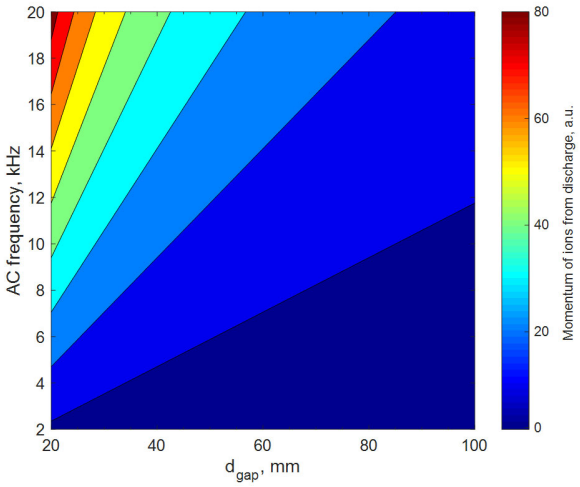

Figure 8. Calculated contours of the momentum of ions estimated from the rate of AC voltage change over time and the drift velocity.

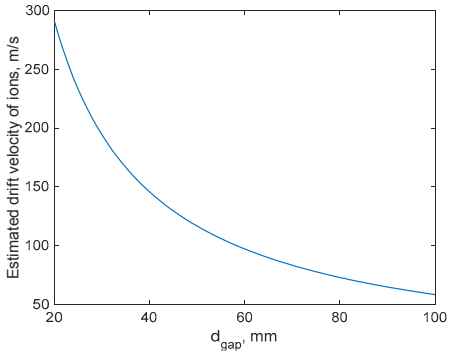

Figure 9. Effect of the gap length on the estimated drift velocity of ions.

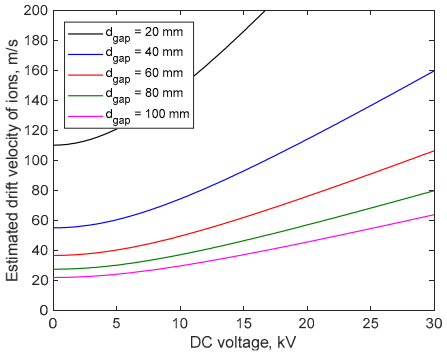

Figure 10. Estimated drift velocity plotted against the DC voltage for various gap lengths, at V_{ac} = 15.6 kV_{pp}.

3.2. Thrust of the induced jet for various AC frequencies

Figure 11 presents the vertical thrust component of the induced jet from the TED plasma actuator for various AC frequencies. Figure 11(a) is the case for the distance between two exposed electrodes (gap length, d_{gap}) was set at 40 mm, and (b) and (c) represent the case for d_{gap} = 60 mm and 80 mm, respectively. To discuss the basic characteristics, we focus on the case of the applied AC voltage was set at V_{ac} = 15.6 kV_{pp} in this paper.

As pointed by the previous research [5], the vertical thrust component starts to rise when the discharge between the electrodes starts at a certain DC voltage. The discharge leads the negative body force at the DC electrode, resulting in the generation of the counter jet to the standard SDBD plasma jet. Once the threshold DC voltage is exceeded, the vertical component of the thrust increases until the maximum DC voltage at which the irregular arc discharge starts between the electrodes. In all cases, the positive vertical thrust, which indicated vertical jet from the surface of the actuator, was observed in the present experimental results.

From figure 11(a) ~ (c), we can observe the effect of the gap length on the thrust characteristics. When d_{gap} is small, the threshold DC voltage to start the counter jet generation is relatively low. For d_{gap} = 40 mm, this threshold voltage corresponds to 14~16 kV, while it becomes >17 kV at d_{gap} = 80 mm. The growth rate of the thrust is relatively large at d_{gap} = 40 mm, then decreases as d_{gap} becomes large.

Then, the effect of the frequency of AC voltage is discussed. From figure 11(a), the difference of the frequency can be observed. At a high AC frequency (f_{ac} = 16 ~ 18 kHz), the threshold DC voltage is small, and the vertical component of the thrust linearly increases at a relatively high rate. At slightly lower (f_{ac} = 13 ~ 15 kHz) frequency, the overall characteristics is same as the high AC frequency cases, however the thrust at the same DC voltage was lowered about 20 %. This is due to the delay of the threshold DC voltage, since the growth rate of the thrust is not changed in this frequency range. On the other hand, at the low frequency (f_{ac} = 4 ~ 7 kHz) the thrust characteristics showed significant change. The threshold voltage did not change largely, however the growth rate of the thrust became small and nonlinear as the frequency was decreased.

The effect of the frequency is moderated as the gap length increases. Even the case d_{gap} = 80 mm, small difference in the thrust curve is observed, and the higher frequency generates higher thrust. However, the growth rate of the thrust is entirely deteriorated, and the difference in the thrust is diminished, as presented in figure 10.

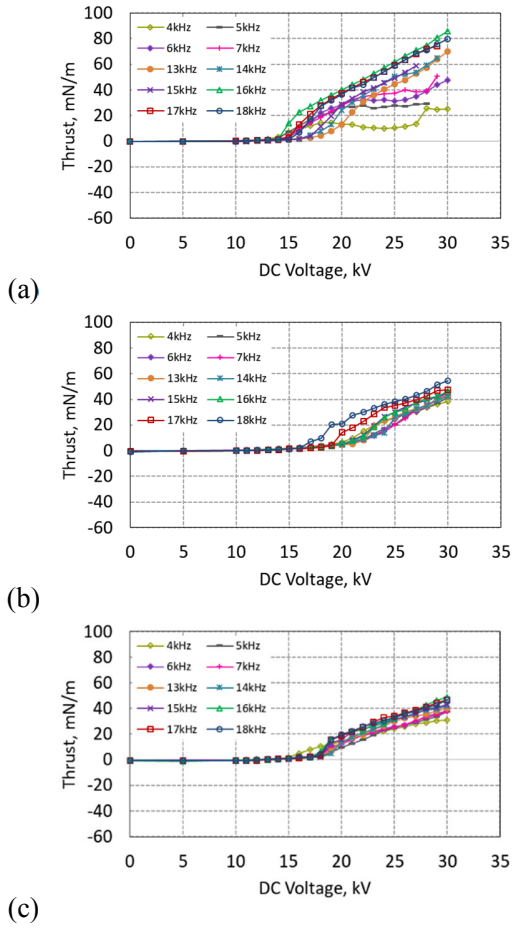

Figure 11. Vertical thrust component versus DC Voltage at V_{ac} = 15.6 kV_{pp} for various AC frequencies: (a) d_{gap} = 40 mm, (b) 60 mm, and (c) 80 mm.

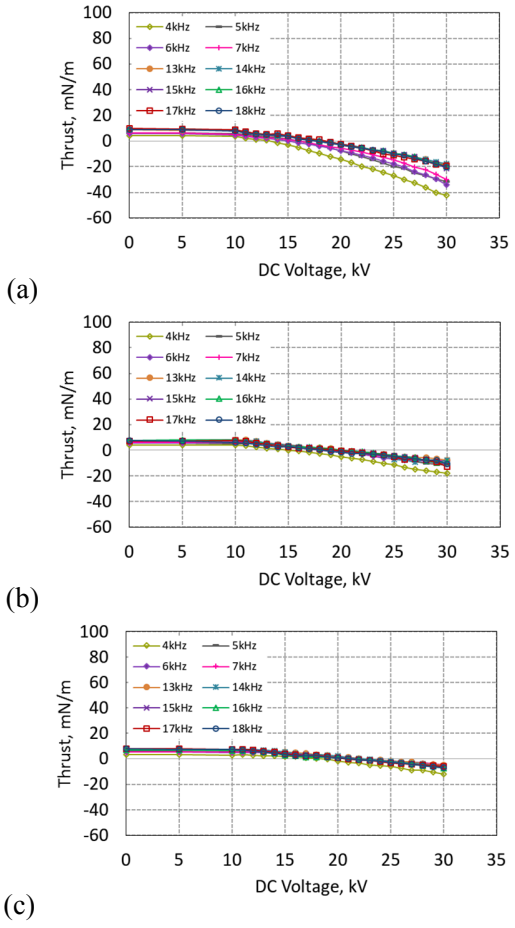

Figure 12. Horizontal thrust component versus DC Voltage at V_{ac} = 15.6 kV_{pp} for various AC frequencies: (a) d_{gap} = 40 mm, (b) 60 mm, and (c) 80 mm.

Figure 12 shows the horizontal component of the thrust of the induced jet from the TED plasma actuator for various AC frequencies. Figure 12(a) ~ (c) represent the case for d_{gap} = 40, 60 and 80 mm, respectively. At V_{dc} = 0, which represents the SDBD condition, the thrust exhibited 7.45 ~ 8.85 mN/m in the current cases. The horizontal thrust decreased and become negative as the counter jet from the DC electrode produced. As expected from the results shown in figure 11, the horizontal thrust component shows that the effect of the gap length is moderated as d_{gap} is increased, as well as for the effect of the frequency.

Figure 13 presents the deflected angle of the thrust vector calculated from figures 11 and 12 versus applied DC voltage. At small DC voltage, the jet is almost parallel to the dielectric surface as SDBD jet. The direction of the induced jet is rapidly changed upward as the DC voltage rise at V_{dc} is from 10 to 20 kV. Once the angle is reached to 90 degrees, the direction shows small change even the DC voltage is increased for the most of the cases.

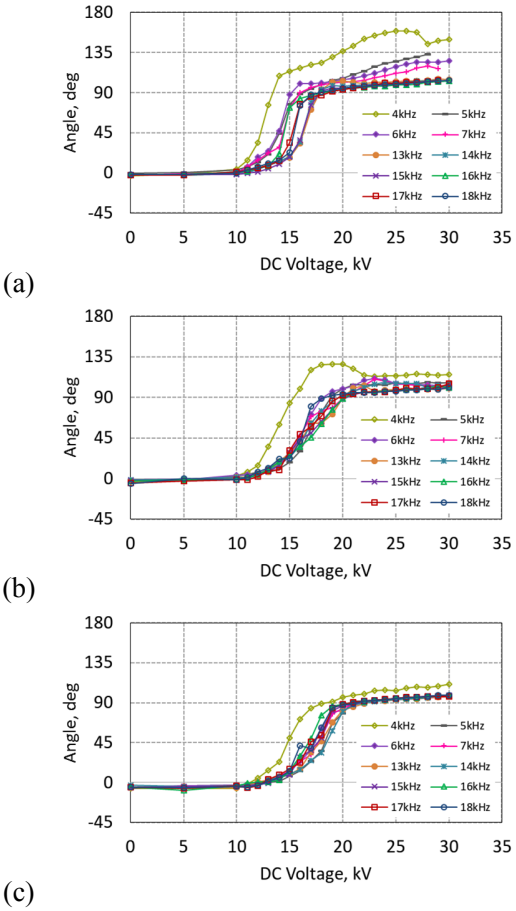

Figure 13. Angle of thrust vector from the wall at V_{ac} = 15.6 kV_{pp}: (a) d_{gap} = 40 mm, (b) 60 mm, and (c) 80 mm.

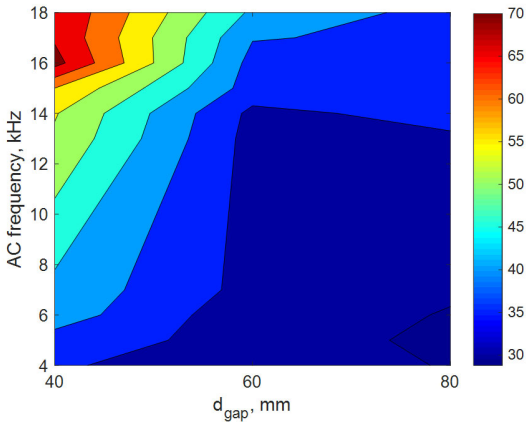

Figure 14. Contour plot of the thrust about d_{gap} and AC frequency at V_{dc} = 27 kV.

The impact of the gap length and the frequency is analyzed with the DC and AC voltage is fixed. Figure 14 shows the same results as in figure 8 as contour map of the thrust at The DC voltage of 27 kV. V_{dc} = 27 kV is the maximum conditions where all of the cases have the data without irregular arc discharge. This again illustrates the effect of the gap length. The impact of the gap length on the thrust becomes significantly small at a large d_{gap}. At a small d_{gap}, the thrust shows rapid increase as the frequency rise. The trend of the contour map of the thrust about these two parameter is quite similar to the estimated momentum shown in figure 8. This analogy indicates that the characteristics of the TED plasma actuator can be predicted from those two physical parameters (the rate of AC voltage change and the drift velocity of ions) and the gap length and the AC voltage frequency affect them as modeled at section 3.1.

Figure 15 shows the total thrust of the induced jet plotted against the power consumption of the driving apparatus for various gap lengths. As expected from the estimation, the input power rises as AC frequency increased, for all gap length cases. Nevertheless, the power efficiency is significantly improved by utilizing the serrated-edge TED plasma actuator, especially when the larger thrust is generated. At this case, the thrust

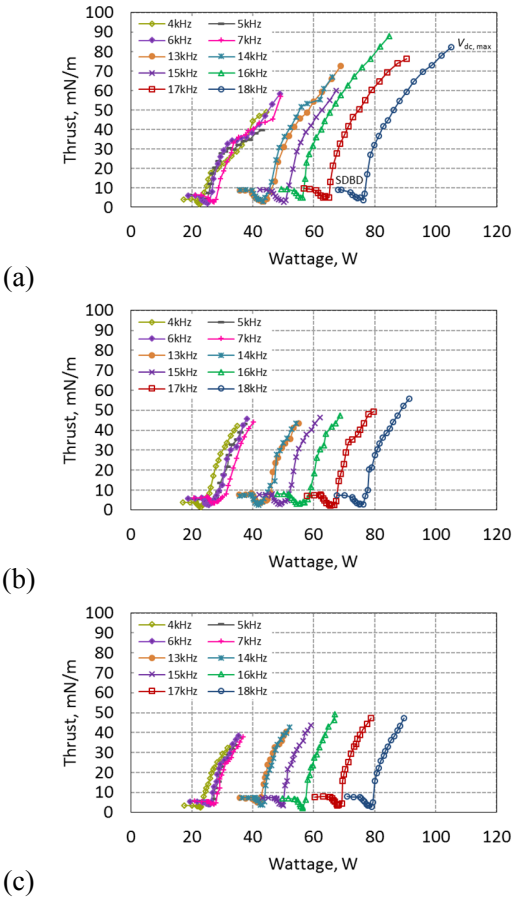

Figure 15. Thrust versus power consumption at $V_{ac} = 15.6\ kV_{pp}$: (a) $d_{gap} = 40$ mm, (b) 60 mm, and (c) 80 mm.

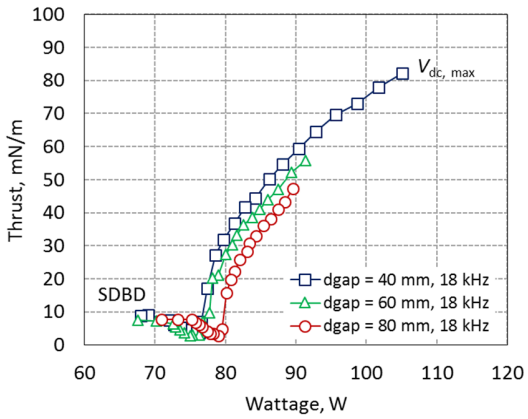

Figure 16. Total thrust versus power consumption at $f_{ac} = 18$ kHz.

becomes 830 percent larger than that of the SDBD plasma actuator, by additional 55 percent of the input power.

Figure 16 compares the total thrust produced as a function of the power consumption for each gap length. All of the cases shows similar curve, as their thrust rapidly rise at a same rate as the power increases at high-thrust regime, at which the peculiar discharge of the trielectrode plasma actuator occurs. The plot also shows that small gap length could produce larger thrust at the same input power. The wattage at the maximum V_{dc} was largely different even at the same DC voltage ($V_{dc} = 30$ kV), however, this condition still shows the highest thrust per unit input power in all of the conditions tested.

4. Summary

The impact of the frequency of the AC voltage and the distance between their exposed electrodes (gap length) on the thrust characteristics of the TED plasma actuator have been investigated experimentally. The induced body force of the serrated TED plasma actuator is investigated on quiescent air. In addition to that, the physical factors that affect the growth of thrust is considered by estimating total momentum of ions from the drift velocity.

From the results of the thrust measurement, the effect of the gap length and the frequency on the thrust characteristics has been clarified. The impact of the gap length on the thrust becomes significantly small at large gap. At small gap, the thrust shows rapid increase as the frequency rise. The power efficiency is significantly improved. The thrust becomes 830 percent larger than that of the SDBD plasma actuator, by additional 55 percent of the input power. The basic characteristics of the TED plasma actuator can be predicted from two physical parameters, the rate of the AC voltage change and the drift velocity of ions, and they are affected by the gap length and the AC voltage frequency.

Acknowledgments
This research was partially supported by KAKENHI (23760771, 15K05797) from JSPS, JAPAN.

References

[1] Corke T C, Post M L and Orlov D M 2007 SDBD plasma enhanced aerodynamics: concepts, optimization and applications *Prog. Aerosp. Sci.* **43** 193–217
[2] Wang J-J, Choi K-S, Feng L-H, Jukes T N and Whalley R D 2013 Recent developments in DBD plasma flow control *Prog. Aerosp. Sci.* **62** 52–78
[3] Matsuno T, Maeda K, Yamada G, Kawazoe H and Kanazaki M 2013 Improvement of Flow Control Performance of Plasma Actuator Using Wind-Tunnel Test Based Efficient Global Optimization *31st AIAA Applied Aerodynamics Conference* 1–10
[4] Sosa R, Artana G, Moreau E and Touchard G 2007 Stall control at high angle of attack with plasma sheet actuators *Exp. Fluids* **42** 143–67
[5] Sosa R, Arnaud E, Memin E and Artana G 2009 Study of the flow induces by a sliding discharge *IEEE Trans. Dielectrics and Electrical Insulation* **16** 305–11
[6] Lago V, Grondona D, Kelly H, Sosa R, Marquez A and Artana G 2009 Sliding discharge optical emission characteristics *IEEE Trans. Dielectrics and Electrical Insulation* **16** 292–8
[7] Matsuno T, Kawaguchi M, Fujita N, Yamada G and Kawazoe H 2012 Jet Vectoring and Enhancement of Flow Control Performance of Trielectrode Plasma Actuator *6th AIAA Flow Control Conference*
[8] Matsuno T, Sugahara M, Koyama J, Fujita N, Yamada G and Kawazoe H 2016 Vectored Jet Control for Trielectrode Plasma Actuator with Serrated Electrode *Trans. Japan Soc. Aeronaut. Sp. Sci. Aerosp. Technol. Japan* **14** Pe_55-Pe_61
[9] Nishida H, Nakai K and Matsuno T 2017 Physical Mechanism of Tri-Electrode Plasma Actuator with Direct-Current High Voltage *AIAA J.* **55** 1852–61